Available online at www.sciencedirect.com
ScienceDirect
International Journal of Pharmaceutics 336 (2007) 122–132
INTERNATIONAL JOURNAL OF PHARMACEUTICS
www.elsevier.com/locate/ijpharm

Solid dispersions of itraconazole and enteric polymers made by ultra-rapid freezing

Kirk A. Overhoff [a], Alejandro Moreno [a], Dave A. Miller [a], Keith P. Johnston [b,**], Robert O. Williams III [a,*]

[a] *College of Pharmacy, University of Texas at Austin, Austin, TX 78712, USA*
[b] *Department of Chemical Engineering, University of Texas at Austin, Austin, TX 78712, USA*

Received 18 August 2006; received in revised form 12 October 2006; accepted 21 November 2006
Available online 26 November 2006

Abstract

The primary objective of the study is to investigate the influence of composition parameters including drug:polymer ratio and polymer type, and particle structure of enteric solid dispersions on the release of ITZ under sink and supersaturated dissolution conditions. Modulated differential scanning calorimetry (MDSC) was utilized to define the level of ITZ miscibility with each polymer. The compositions were completely miscible at 60% ITZ for both polymers and as high as 70% in HP-55. High potency composition glass transition temperatures (T_g) correlated with predicted T_g's from the Gordon–Taylor equation, however, recrystallization exotherms revealed pure amorphous regions indicating that phase separation occurred during particle formation. Furthermore, *in vitro* studies including X-ray powder diffraction (XRD), scanning electron microscopy (SEM), surface area analysis (BET), and dissolution were performed to determine differences between low potency (completely miscible) and high potency (partially miscible) compositions. Dissolution studies on low potency ITZ compositions revealed that miscibility plays an active role in ITZ release under sink conditions, and square root diffusion through the enteric polymer is observed. Supersaturated dissolution profiles revealed high potency compositions had maximum saturation levels ($C/C_{eq_{max}}$) between 10.6- and 8-times equilibrium solubility, but had higher cumulative extents of supersaturation, compared to low potency compositions which had $C/C_{eq_{max}}$ values of 15–19.6. However, these low potency compositions rapidly precipitated leading to significantly lower AUCs ($p < 0.05$). The change in the miscibility of the solid dispersion had a pronounced effect of drug release (sink) while differences in potency influenced supersaturated dissolution profiles.

Keywords: Particle engineering; Amorphous; Supersaturation; Nanoparticle; Enteric polymer; Dissolution model

1. Introduction

Itraconazole (ITZ) is a broad spectrum triazole antifungal with pH dependent solubility. It is a weak base ($pK_{a_1} = 3.7$) and is more soluble in the gastric environment of the stomach compared to the more neutral pH of the other parts of the small intestine (Peeters et al., 2002). Intuitively, it may appear that the likely site of absorption would be in the acidic environment of the stomach. In fact, immediate release systems including both oral and pulmonary formulations have been developed to try and improve the overall bioavailability by increasing the apparent solubility of ITZ (Frei, 2003; Hoeben et al., 2006; McConville et al., 2006; Sinswat et al., 2005). Pulmonary delivery has the advantage of bypassing first pass metabolism and can deliver both local and systemic treatment, but traditionally has lower patient compliance compared to oral delivery. Major limitations to oral delivery include variable gastric emptying times, which can lead to variable absorption rates and food effects, which can alter the pH leading to further variability. Likewise the surface area (SA) of the stomach available for absorption is small relative to other absorption sites in the GI tract. In fact, investigation of the stomach lining reveals epithelial layers which continually shed cells limiting absorption (Mayersohn, 2002). However, the intestinal surface is composed of microscopic finger-like projections known as villi and microvilli which increase the

* Corresponding author at: College of Pharmacy (Mailstop A1920), University of Texas at Austin, Austin, TX 78712-1074, USA. Tel.: +1 512 471 4681; fax: +1 512 471 7474.
** Corresponding author. Tel.: +1 512 471 4617; fax: +1 512 475 7824.
E-mail addresses: kpj@che.utexas.edu (K.P. Johnston), williro@mail.utexas.edu (R.O. Williams III).

0378-5173/$ – see front matter © 2006 Elsevier B.V. All rights reserved.
doi:10.1016/j.ijpharm.2006.11.043

absorptive surface area of the small intestine 600-fold (>170 m^2) (Sherwood, 2004) making it an excellent site for absorption. However, as ITZ enters the small intestines, the change in pH has the potential to precipitate ITZ that was dissolved in the stomach, slowing the absorption process and decreasing bioavailability. In addition, any undissolved particles would remain insoluble with a pH above the pK_a. Amorphous solid dispersions containing enteric polymers could overcome these limitations by (1) delaying dissolution until the compound enters the intestines preventing premature precipitation of the ITZ and (2) increasing the apparent solubility at higher pH to increase the driving force for absorption. Amorphous drugs can achieve a supersaturated state due to their low heat of fusion (Yoshihashi et al., 2000). Hancock and Parks have shown that amorphous indomethacin has a 2.5-times increase in apparent solubility compared to its crystalline counterpart (Hancock and Parks, 2000) while up to a 25-times increase in solubility has been reported for tacrolimus and diacetylmidecamycin (Yamashita et al., 2003; Sato et al., 1981). However, these supersaturated solutions are thermodynamically unstable and will precipitate and return to the equilibrium state over time. Therefore, a stabilizing polymer must be included to extend the time the compound remains supersaturated. These polymers are able to prevent recrystallization or particle growth in solution through hydrogen-bonding (Raghavan et al., 2001a,b) or adsorbing on the surface of solid particles blocking the addition of other solute onto the surface (Sung et al., 2002; Mackellar et al., 1994; Suzuki and Sunada, 1998).

Modified release systems including delayed release systems are used to target delivery of the API within a specific section of the GI tract or when gastric degradation can severely limit the effectiveness of the API. One common approach is to coat the surface of the delivery system (microspheres, tablets, beads/pellets, etc.) with a gastro-resistant polymer, which often displays pH dependent solubility. These polymers typically contain functional groups, which ionize at specific pH values, allowing for targeted delivery of the API to certain sections of the GI tract and are often referred to as enteric polymers. Hasegawa et al. (1984) were the first to develop solid dispersions comprising a binary mixture of a poorly water soluble API, nifedipine, and an enteric polymer. A variety of technologies have been employed to develop these enteric solid dispersions such as traditional melt dispersion (Hasegawa et al., 1988), hot melt extrusion/spheronization (Varshosaz et al., 1997; Nakamichi et al., 2002), anti-solvent precipitation (Sertsou et al., 2003), solvent evaporation (Kohri et al., 1999; Kondo et al., 1994), and spray drying (Takeuchi et al., 1987). A novel technique based on the aerosol flow reactor has also been used to produce solid dispersions (Eerikainen et al., 2004b). Oral absorption of poorly water soluble compounds has been achieved using these enteric solid dispersions (Kai et al., 1996; Kohri et al., 1999) particularly since they can delay dissolution and supersaturation until the API reaches the upper small intestine (Kondo et al., 1994). To date, high potency compositions with desirable delayed release properties have not been achieved as a result of miscibility limitations between the API and the enteric polymer.

The objective of the study is to investigate the influence of composition parameters including drug:polymer ratio and polymer type, and particle structure of enteric solid dispersions on the release of ITZ under sink and supersaturated dissolution conditions. Solid dispersions containing ITZ and an enteric polymer were produced using the ultra-rapid freezing (URF) process. The URF process is shown to create amorphous API allowing for supersaturation, while the enteric polymer protects the ITZ from premature dissolution in the acidic environment and prevents particle growth in higher pH environments. Since drug release for modified release systems is dependent on the polymer release characteristics, the degree of miscibility may be expected to play a key role on dissolution. To define the level of ITZ miscibility with the enteric polymers, MDSC was performed on varying ITZ potency URF micronized powders. Once ITZ miscibility limits were established, the effects of ITZ potency, enteric polymer type, and % total solids in the feed on *in vitro* dissolution were assessed.

2. Materials and methods

2.1. Materials

Itraconazole (ITZ) was purchased from Hawkins Chemical (Minneapolis, MN, USA). The enteric polymers hydroxypropylmethyl cellulose phthalate NF (HP55) and Eudragit L100-55 (L100-55) were purchased from Shin Etsu Chemical (Tokyo, Japan) and Röhm GmbH (Darmstadt, Germany), respectively. Histological grade 1,4-dioxane, 99%+, was purchased from Sigma–Aldrich (St. Louis, MO, USA). HPLC grade acetonitrile (ACN) was purchased from EMD chemicals (Gibbstown, NJ, USA). Diethanolamine, hydrochloric acid and tribasic sodium phosphate was purchased from Fisher chemicals (Fair Lawn, NJ, USA). Polysorbate 20 was purchased from Spectrum Chemical (Gardena, CA, USA).

2.2. Preparation of URF powders

ITZ and the pH-dependent polymer were dissolved in an appropriate amount of 1,4-dioxane and rapidly frozen using the URF apparatus. The API/polymer solutions were applied to a cryogenic solid substrate cooled to −60 °C, collected, and lyophilized using a VirTis Advantage benchtop tray lyophilizer (The VirTis Company, Inc., Gardiner, NY, USA).

2.3. Modulated differential scanning calorimetry (MDSC)

Samples in the range of 8–10 mg of processed and bulk powders were added to crimp sealed aluminum pans and measured on a TA Instruments model 2920 MDSC (New Castle, DE, USA). Samples were heated at a rate of 2 °C/min from 30 to 200 °C at a modulating oscillatory frequency of 0.21 °C/min. Samples were purged with nitrogen gas at 150 mL/min. Glass transition temperatures were measured at the midpoint of the step transition. The MDSC was calibrated using an indium standard.

2.4. True density measurements

True density was measured using the true density of the pure amorphous ITZ and enteric polymer was determined using helium pycnometry (Micrometrics AccuPyc 1330 pycnometer; Norcross, GA). URF processed pure components were immediately tested after removal from the lyophilizer to limit water adsorption and placed in a sample cup and purged 20 times at 19.85 psi followed by six analytical runs at 19.85 psi. The equilibration rate was 0.0050 psi/min. Measurements were performed in triplicate.

2.5. Scanning electron microscopy (SEM)

The powder samples were sputter coated using a model K575 sputter coater (Emitech Products, Inc., Houston, TX, USA) with gold–palladium for 35 s and viewed using a Hitachi S-4500 field emission scanning electron microscope (Hitachi High-Technologies Corp., Tokyo, Japan). An accelerating voltage of 5 kV was used to view the images. All SEMs pictured were representative of the entire sample.

2.6. Sink dissolution testing

Dissolution testing was performed on the URF powder samples using a USP 25 Type II paddle apparatus model VK7000 (Varian, Inc., Cary, NC, USA). An equivalent of 1 mg ITZ was pre-wetted with 0.075% Polysorbate 20 in de-ionized water and added to 900 mL of 0.1N HCl (pH 1.2) dissolution media. The dissolution media was maintained at $37.0 \pm 0.2\,^{\circ}C$ and the paddle speed was maintained at 100 rpm throughout the testing period.

Samples (5 mL) were withdrawn at 15, 30, 45, 60, 90 and 120 min time points, filtered using a 0.20 μm Whatman nylon filter (Clifton, NJ, USA), diluted with HPLC grade ACN, and analyzed using a Shimadzu LC-10 liquid chromatograph (Shimadzu Corporation, Kyoto, Japan) equipped with an Alltech ODS-2 5 μm C_{18} column (Alltech Associates, Inc., Deerfield, IL, USA). A mobile phase of ACN:water:diethanolamine (70:30:0.05) at 1 mL/min eluted the ITZ peak at 5.5 min and absorbance was measured at wavelength $\lambda = 263$ nm.

2.7. Supersaturation dissolution testing

Dissolution testing was performed on the URF powder samples using a USP 25 dissolution apparatus model VK7000 (Varian, Inc., Cary, NC, USA). Dissolution was conducted according to USP enteric test method A for delayed release dosage forms using 100 mL glass dissolution vessels and stirred with appropriate small paddles. An equivalent of 8.8 mg ITZ (20X ITZ equilibrium solubility) was pre-wetted with 5 mL 0.008% Polysorbate 20 in 0.1N HCl and added to 70 mL 0.1N HCl (75 mL total). The dissolution media was maintained at $37.0 \pm 0.2\,^{\circ}C$ and the paddle speed was maintained at 50 rpm throughout the testing period. After 2 h, 0.2 M tribasic sodium phosphate (Na_3PO_4) containing 0.28% sodium dodecyl sulfate was equilibrated to $37.0 \pm 0.2\,^{\circ}C$ and added to the dissolution vessels. Therefore, the final SDS concentration was 0.07%, which was determined to give equal equilibrium solubilities of ITZ in both pH environments. For each time point, 3 mL of medium was withdrawn and filtered using a 0.20 μm nylon filter, diluted with HPLC grade ACN, and analyzed according to the HPLC method outlined above.

2.8. X-ray diffraction (XRD)

The X-ray diffraction pattern of the SFL powders were analyzed using a model 1710 X-ray diffractometer (Philips Electronic Instruments, Inc., Mahwah, NJ, USA). Data were collected using primary monochromated radiation (Cu $K\alpha_1$, $\lambda = 1.54056$ Å), a 2θ step size of 0.05 and a dwell time of 1.0 s per step.

2.9. BET specific surface area analysis

Specific surface area was measured using a Nova 2000 v.6.11 instrument (Quantachrome Instruments, Boynton Beach, FL, USA). Weighed powder was added to a 12 mm Quantachrome bulb sample cell and degassed for a minimum of 3 h. The sample was then analyzed by the NOVA Enhanced Data Reduction Software v. 2.13 using the BET theory of surface area.

2.10. Statistical analysis

One-way analysis of variance (ANOVA, $\alpha = 0.05$) was used to determine statistically significant differences between results. Results with p-values <0.05 were considered statistically significant. Post hoc analysis using Tukey's honestly significant difference (HSD) test was performed after analysis to determine individual differences between compositions. Mean differences greater than the HSD were deemed statistically significant.

3. Results

3.1. ITZ miscibility in URF micronized powders

MDSC was used to determine the level of ITZ, which could be added to the mixture before reaching phase separation and partial miscibility. Fig. 1a shows the MDSC profiles for increasing levels of ITZ in HP-55 (every 10% up to 80% ITZ) prepared via the URF process from a feed solution of 2.0%. Pure amorphous ITZ manufactured by the URF process was also included as a reference. To investigate if the nucleation process during rapid freezing and particle formation can enhance the miscibility of ITZ and HP-55, MDSC was also performed on the ITZ:HP-55 URF powders from 0.2% total solids loading. Profiles for the 0.2% loading were identical to those presented in Fig. 1b and the data is not shown. For samples with ITZ lower than 60% ITZ, no melting endotherms were detected and only a single glass transition (T_g) was detected. T_g decreased with increasing ITZ potency. Upon increasing the ITZ potency to 70%, a slight melting endotherm was detected, while increasing the ITZ potency to 80% caused a large melting endotherm for both feed concentrations. Interestingly, only one single T_g was detected at 70% ITZ

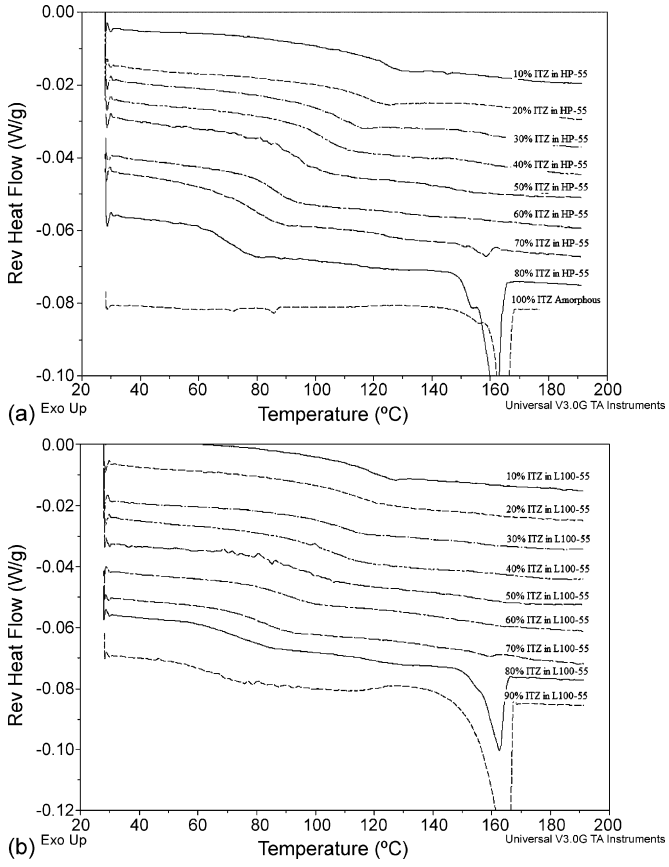

Fig. 1. Reverse heat MDSC profile for increasing potencies of URF micronized compositions containing (a) ITZ:HP-55 manufactured from 2.0% total solids feed and (b) ITZ:L100-55 manufactured from 0.2% total solids feed. Heat flow values are relative for comparison purposes.

and two T_gs were detected at 80% ITZ (2% only). The melting point for the 70% and 80% ITZ compositions were measured at 158.4 and 162.7 °C, respectively, which are lower than the melting point of micronized crystalline ITZ (166.8 °C) which was measured separately (data not shown). The melting point depression is thought to occur from the polymer HP-55, which is estimated to melt at 150 °C. Fig. 1b shows the MDSC profiles for the ITZ:L100-55 binary mixtures manufactured from the URF process. Increasing levels of ITZ in L100-55 (every 10%) were analyzed to determine if phase separation occurs. Just as in the previous figures, a melting endotherm was detected for ITZ potencies greater than or equal to 70%. In addition, only a single T_g was detected for all potencies and decreased with increasing levels of ITZ.

Compositions containing 70% ITZ or greater displayed a recrystallization exotherm when analyzing total heat flow MDSC profiles. Examples of these recrystallization exotherms can be seen in Fig. 2. Compositions containing 70% ITZ in HP-55 showed a slight melting endotherm, but did not produce the recrystallization exotherm associated with pure amorphous ITZ. The recrystallization endotherm is present when the potency is increased to 80%. For the ITZ:L100-55, a small recrystallization endotherm appears at 70% ITZ and increases as potency increases. Likewise, as the recrystallization endotherm

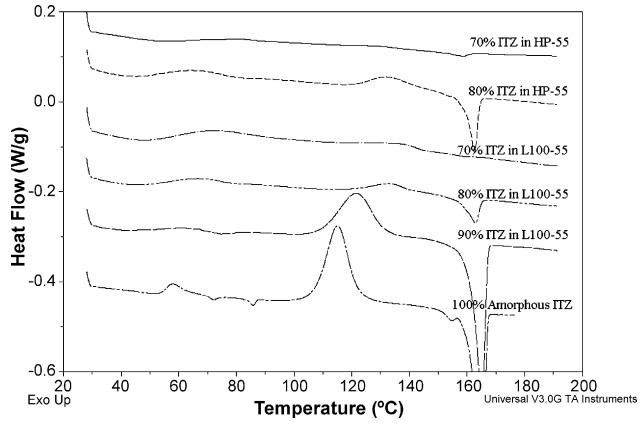

Fig. 2. Total heat flow MDSC for high potency URF micronized ITZ:HP-55 (2%) and ITZ:L100-55 (0.2%) powders. Heat flow values are relative for comparison purposes.

increases, the melting endotherm increases as a result of the melting recrystallized ITZ.

The Gordon–Taylor equation is used to predict the T_g's for binary mixtures (T_{g12}) of polymers and has also been applied to estimate the T_g for API (small molecule) and polymer mixtures. Briefly, the Gordon–Taylor equation is as follows:

$$T_{g12} = \frac{w_1 T_{g1} + K w_2 T_{g2}}{w_1 + K w_2} \quad (1)$$

where T_{g1} and T_{g2} are the glass transition temperatures of the pure amorphous components and K is a constant determined by the Simha–Boyer rule:

$$K \cong \frac{\rho_1 T_{g1}}{\rho_2 T_{g2}} \quad (2)$$

where ρ_1 and ρ_2 are the true densities of the pure amorphous components. The measured T_g's for the increasing potencies of ITZ were plotted against the estimated T_g's from the Gordon–Taylor equation for each of the ITZ:polymer binary mixtures as depicted in Fig. 3a and b. The predicted T_g's values were constructed by first measuring the T_g's and true density

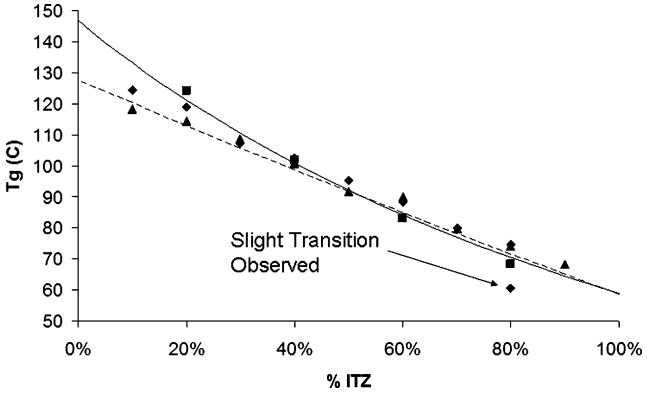

Fig. 3. Measured glass transition (T_g) temperatures for increasing potencies of URF micronized compositions plotted vs. theoretical T_g calculated from Gordon–Taylor equation: ITZ:HP-55 from 2.0% feed (♦), 0.2% feed (■), theoretical ITZ:HP-55 (solid line), ITZ:L100-55 from 0.2% feed (▲), theoretical ITZ:L100-55 (dashed line).

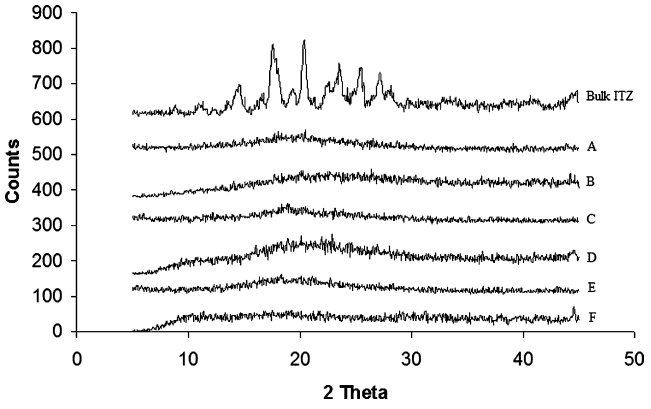

Fig. 4. X-ray diffraction profiles for URF micronized powders containing binary mixtures of ITZ and a enteric polymer (% total solids in feed): (Bulk ITZ) bulk ITZ, (A) 4:1HP55 (2%), (B) 1:4HP55 (2%), (C) 4:1HP55 (0.2%), (D) 1:4HP55 (0.2%), (E) 4:1L100-55 (0.2%), (F) 1:4L100-55 (0.2%).

of the pure amorphous components using MDSC and helium pycnometry, respectively. The measured T_g's for amorphous ITZ, HP-55, and L100-55 are 59, 147, and 128 °C, respectively. The true densities were measured at 1.37, 1.75, and 1.32 g/cm^3, respectively, and agree closely with literature values (Rowe et al., 2003). Fig. 3a plots the T_g's for the ITZ:HP-55 binary mixtures from both the 2.0% and 0.2% total solids feed solutions. Interestingly, all potencies revealed a very close correlation with the predicted T_g. At 80% ITZ, two T_g's exist for the 2.0% total solids loading (as stated above) and the measured values are 74.7 and 60.5 °C, the latter in good agreement with pure amorphous ITZ at 59 °C. Measured T_g values for the powders produced from a 0.2% feed solution also closely agreed with the predicted values at all potencies. In Fig. 3b, the measured T_g's for the ITZ:L100-55 binary mixtures are shown. Again, measured T_g's for all potencies up to 90% ITZ were very close to T_g's predicted by the Gordon–Taylor equation.

3.2. *In vitro analysis of low and high potency URF micronized binary mixtures*

In order to determine the effect of ITZ potency on the *in vitro* performance of the powders, low (1:4 ITZ:polymer ratio) and high potency ITZ (4:1 ITZ:polymer ratio) compositions were manufactured via the URF process. For compositions containing HP-55, two total solids feed solution concentrations (0.2% and 2.0%) were examined. Compositions containing L100-55 were manufactured from 0.2% total solids feed solutions due to solubility limitations of this polymer in the feed solvent. For convenience, the compositions will be referred to by the ITZ:polymer ratio (1:4 or 4:1), followed by the polymer type (HP55 or L100-55) and concluding with the % total solids in the feed (2% or 0.2%).

The crystallinities of URF processed powders were examined using XRD and the profiles are depicted in Fig. 4. From the diffraction profile, the characteristic ITZ peaks (most intense) used for determining crystallinity of the URF processed samples are located at 17.45 and 17.95 (doublet), 20.30, and 23.45 two theta degrees. XRD profiles for the all URF micronized powders lacked the diffraction peaks associated with crystalline ITZ implying the samples contained amorphous ITZ.

Scanning electron micrographs were taken to determine the surface morphology of each of the URF micronized compositions at 30,000× magnification (Fig. 5a–f). Close inspection of the morphology of 4:1HP55 (2%) in Fig. 5a reveals aggregated nanoparticles arranged in a matrix composed of macropores on the order of 800 nm leading to a powder. 1:4HP55 (2%) (Fig. 5b) is composed of pores ranging from 50 to 200 nm in diameter; however, the matrix surface appears smooth and flat. Likewise, 4:1HP55 (0.2%) (Fig. 5c) which contains a high level of ITZ (80%) appears different from 1:4HP55 (0.2%) (Fig. 5d) which contains low levels of ITZ (20%). 4:1HP55 (0.2%) appears to display smooth thread-like structures over a majority of the particle surface, while spherical nanoparticles filled in the rest of the areas. A few of these nanoparticle regions can be seen on the left side and bottom region of the SEM. 1:4HP55 (0.2%) revealed regions of clearly defined nanoparticles (∼100 nm in diameter) but also displayed larger particles (>600 nm) with smooth surfaces. Finally, both 4:1L100-55 (0.2%) (Fig. 5e) and 1:4L100-55 (0.2%) (Fig. 5f) which were composed of ITZ and L100-55 both displayed nanoparticles which appear to be >100 nm in diameter. These micrographs suggest that the surface morphologies are strongly influenced by the amount of polymer present in the feed. For example, while Fig. 5a was composed of 2.0% solids only 20% was polymer leading to nanoparticle formation. Subsequently, lower solids loadings reduced the amount of polymer present regardless of the potency and also resulted in nanoparticles. However, when low ITZ potency is combined with high solids loadings (maximum amount of polymer present, 1:4ITZ:HP55 (2%)) a porous matrix resulted (Table 1).

The specific surface areas of the URF micronized powders (Table 1) were very high and ranged from 19.1 to 122 m^2/g. 4:1HP55 (2%) which was composed of aggregated nanoparticles had a measured surface area of 54.2 m^2/g while its lower potency counterpart 1:4HP55 (2%) had a measured surface area of 19.1 m^2/g. The high polymer levels prevented nanoparticle formation leading to a porous matrix structure and could be a reason for the lower surface area. While this value was lower than those of all other compositions, it still represents a 4.5-fold increase in surface area over micronized ITZ. The compositions which displayed nanoparticles in the SEM also had high surface areas of greater than 57.3 m^2/g with 1:4L100-55 (0.2%) having the highest measured surface area of 122 m^2/g. Interestingly, both compositions containing L100-55 had larger surface

Table 1
Specific surface area for URF micronized powders containing ITZ and an enteric polymer, HP-55 or L100-55

Composition	Surface area (m^2/g)
1:4HP55 (2%)	19.1
1:4HP55 (0.2%)	61.8
1:4L100-55 (0.2%)	122
4:1HP55 (2%)	54.2
4:1HP55 (0.2%)	57.4
4:1L100-55 (0.2%)	79.9
Bulk ITZ	4.22

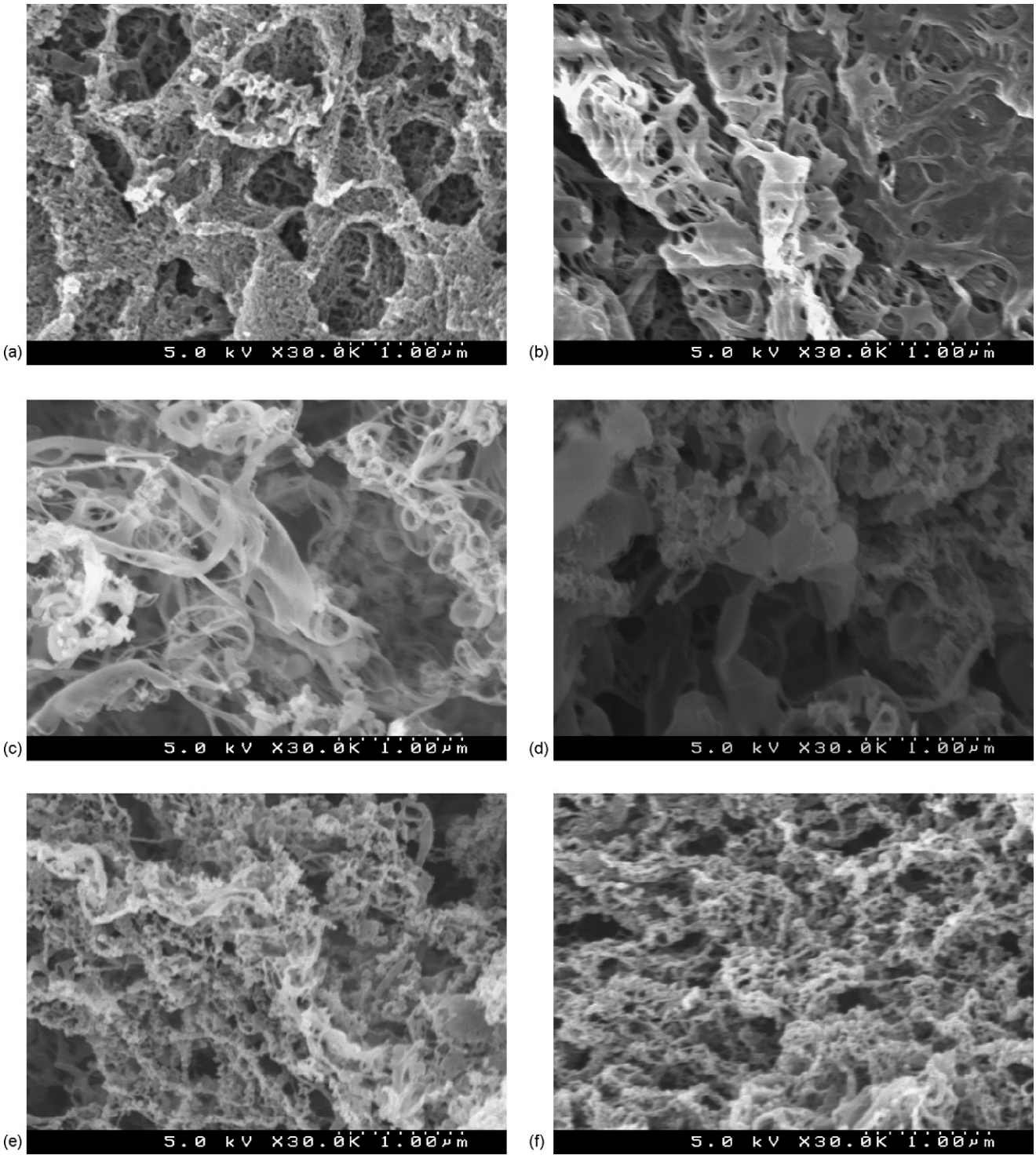

Fig. 5. Scanning electron micrographs of URF micronized powders containing binary mixtures of ITZ and a enteric polymer: (a) 4:1HP55 (2%), (b) 1:4HP55 (2%), (c) 4:1HP55 (0.2%), (d) 1:4HP55 (0.2%), (e) 4:1L100-55 (0.2%), (f) 1:4L100-55 (0.2%).

areas compared to the compositions containing HP-55 (4:1HP55 (0.2%) and 1:4HP55 (0.2%)).

Sink dissolution studies in 0.1N HCl were performed to investigate the effect of potency on drug release. All URF micronized powders were compared to crystalline micronized ITZ which was 65% dissolved after 2 h. The dissolution profiles in Fig. 6a–c show that as potency increases, the rate and cumulative release increases, with 4:1HP55 (2%) having the most ITZ (68.8%) released after 2 h. In the first 30–45 min the slope is particularly large for the high potency samples. Here localized regions of pure amorphous ITZ could exist and be exposed to the dissolution medium creating a burst effect. After 45 min the ITZ release reaches an asymptote. Although all URF micronized powders lacked any crystalline ITZ according to XRD, the total

Table 2
Diffusion modeling correlation and diffusion coefficients for dissolution of URF micronized powders

Composition	Higuchi correlation coefficient (R^2)	Higuchi dissolution constant (K_h)	Calculated diffusion coefficient (D_m) from simplified Higuchi model (1×10^{-13} cm^2/min)
1:4HP55 (2%)	0.991	0.118	1.88
1:4HP55 (0.2%)	0.991	0.045	0.273
1:4L100-55 (0.2%)	0.990	0.011	0.017
4:1HP55 (2%)	0.939	–	–
4:1HP55 (0.2%)	0.922	–	–
4:1L100-55 (0.2%)	0.837	–	–

amount of ITZ released was never higher statistically than for crystalline ITZ, despite the amorphous morphology and considerably higher surface areas. Low ITZ potency compositions released very little ITZ into solution ranging from 12.9 to 27.5% dissolved ITZ after 2 h. The dissolution data were modeled using the simplified Higuchi model to describe diffusional drug release kinetics. Fig. 7a and b show the Higuchi plots for the low potency and high potency compositions, respectively. Qt is the amount of ITZ dissolved per unit area based on the surface area of the powders. In addition, the correlation coefficients (R^2), Higuchi dissolution constants (K_h), and the diffusion coefficients (D) for the low potency compositions are listed in Table 2 (Fig. 8).

Dissolution studies were also performed under supersaturated conditions (20-times the crystalline ITZ equilibrium solubility) to determine the maximum concentrations, and the cumulative supersaturation, which depends both upon dissolution of the powder and the ability of the enteric polymers to inhibit precipitation of ITZ. The dissolution studies were conducted according to the USP XXV enteric test method A, and the results are given in Fig. 8. After 2 h in acidic media, aliquots were removed and the ITZ concentrations were determined. Table 3 lists the percentage of total ITZ added which dissolved within the first 2 h. All values were lower than those which were calculated under sink conditions with 4:1HP55 (2%) having the highest release (23.8%; 6.6-times) and 1:4L100-55 (0.2%) having the lowest % release (5.3%; 1.4-times). Upon addition of the buffer an increase in supersaturation was observed for all

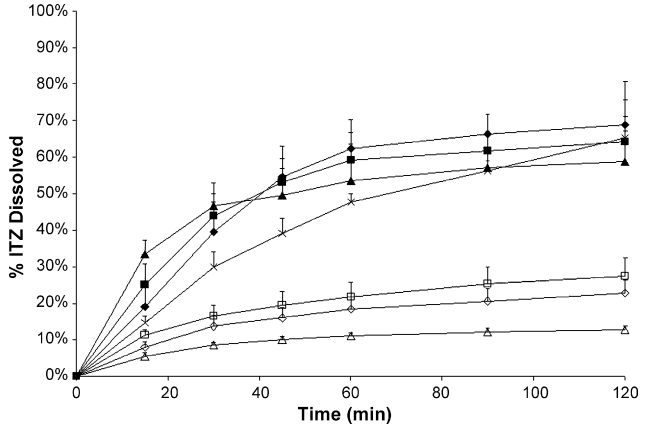

Fig. 6. Sink dissolution profiles of URF micronized powders containing binary mixtures of ITZ and enteric polymer conducted in 0.1N HCl: 4:1HP55 (2%) (♦), 1:4HP55 (2%) (◊), 4:1HP55 (0.2%) (■), 1:4HP55 (0.2%) (□), 4:1L100-55 (0.2%) (▲), 1:4L100-55 (0.2%) (△), bulk crystalline ITZ (×).

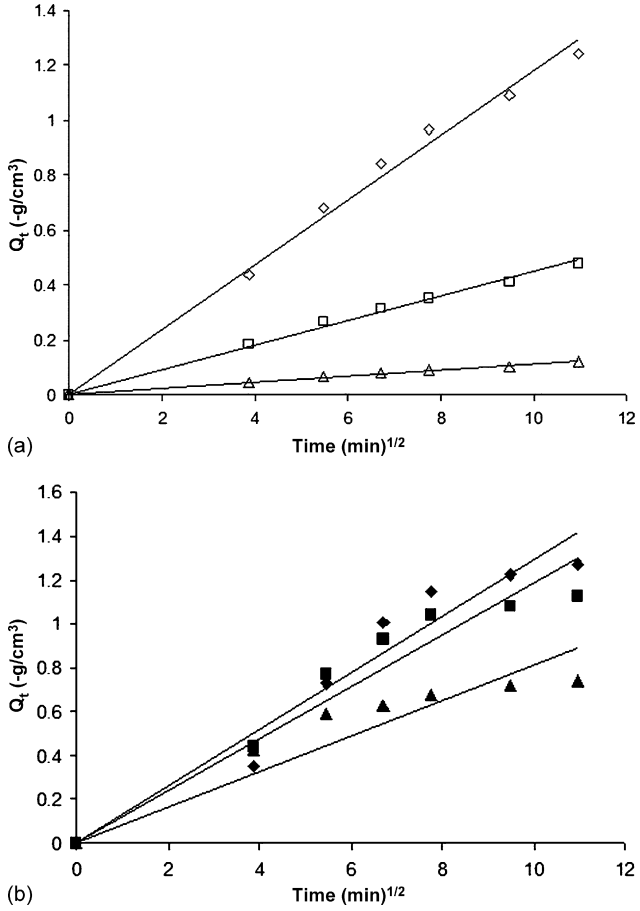

Fig. 7. (a) Higuchi diffusion model fitting of URF micronized powders (a) 1:4HP55 (2%) (◊), 1:4HP55 (0.2%) (□), 1:4L100-55 (0.2%) (△); (b) 4:1HP55 (2%) (♦), 4:1HP55 (0.2%) (■), 4:1L100-55 (0.2%) (▲).

Table 3
Supersaturation data for URF micronized powders containing ITZ and enteric polymer

Composition	% dissolved after 2 h in acidic media[a]	$C/C_{eq_{max}}$	AUC_{ss} (mg min/mL)[b]
1:4HP55 (2%)	14.62 ± 0.63	19.67	17.58 ± 1.31
1:4HP55 (0.2%)	14.14 ± 1.63	17.45	22.41 ± 1.21
1:4L100-55 (0.2%)	5.26 ± 0.62	15.20	22.93 ± 3.21
4:1HP55 (2%)	23.85 ± 0.99	10.68	33.11 ± 2.02
4:1HP55 (0.2%)	14.49 ± 1.09	8.44	37.97 ± 1.08
4:1L100-55 (0.2%)	14.94 ± 1.14	9.27	35.45 ± 2.50

[a] Percent of total ITZ dissolved in gastric medium after 2 h under supersaturated conditions (based on weight added).
[b] Area under curve at supersaturated conditions calculated via trapezoidal rule.

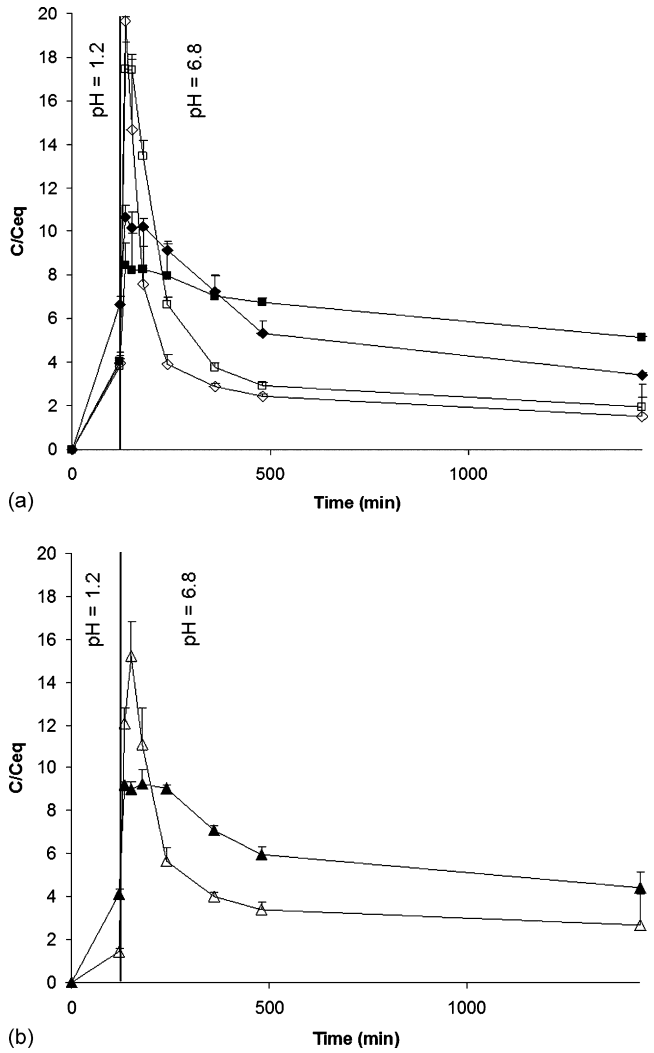

Fig. 8. Supersaturation dissolution profiles of URF micronized powders containing binary mixtures of ITZ and enteric polymer conducted in 0.1N HCl for 2 h and addition of 0.2 M Na_3PO_4 with SDS (final SDS concentration = 0.07%; USP enteric test method A): (a) 4:1HP55 (2%) (♦), 1:4HP55 (2%) (◊), 4:1HP55 (0.2%) (■), 1:4HP55 (0.2%) (□), (b) 4:1L100-55 (0.2%) (▲), 1:4L100-55 (0.2%) (△).

compositions as the enteric polymer dissolved and released the amorphous ITZ within the polymer leading to the maximum extent of supersaturation ($C/C_{eq_{max}}$) for all URF compositions. It was also observed that the degree of supersaturation increase was strongly dependent on the level of polymer in the composition. Low potency ITZ compositions had the highest $C/C_{eq_{max}}$ 15 min after the buffer was added with 1:4HP55 (2%) having the highest measured $C/C_{eq_{max}}$ value of 19.7X. For high potency ITZ compositions, the supersaturation increased after addition of the buffer, with 4:1HP55 (2%) having the highest measured $C/C_{eq_{max}}$ value at 10.7-times equilibrium solubility. However, the supersaturation levels were not as high as those of the low potency compositions.

The supersaturation profiles also indicate that the compositions which achieved a high $C/C_{eq_{max}}$ were also subject to greater subsequent losses in supersaturation, regardless of the stabilizing polymer. In addition, for compositions with a smaller $C/C_{eq_{max}}$, smaller amounts of subsequent precipitation were observed. To place the results in further perspective, the cumulative extent of supersaturation (AUC) was calculated as the area-under-the-supersaturation-curve, as listed in Table 3. High potency URF compositions had significantly higher ($p < 0.05$) AUCs ranging from 33.1 to 38.0 mg min/mL compared to the low potency URF compositions which had AUCs ranging from 17.6 to 22.9 mg min/mL. Further analysis revealed that there were also significant differences in AUC versus the total solids loading for both high and low potencies. The 1:4L100-55 (0.2%) sample has a significantly higher ($p < 0.05$) AUC than 1:4HP55 (0.2%) indicating that L100-55 is able to maintain supersaturation of ITZ longer than HP-55.

4. Discussion

4.1. ITZ miscibility in pH dependent polymer binary mixtures

For immediate release systems, Craig et al. described the mechanism for API release from solid dispersions containing water-soluble polymers (Craig, 2002). They concluded that when the API was dispersed within the polymer on a molecular level (i.e. solid solution) API release was carrier mediated. However, if localized regions of pure API existed (i.e. solid dispersion) and were sufficiently large, dissolution of the API may also be API mediated. In addition, Six et al. investigated the effect of ITZ miscibility within water-soluble polymers to determine the effect of miscibility on dissolution rate (Six et al., 2002, 2004). The results suggest that for immediate release systems, ITZ miscibility within a polymer carrier is not critical to achieve rapid dissolution rates. In fact, both the carrier, in this case, Eudragit® E100, and the physical state of the ITZ contribute to the dissolution rate. In other words, the E100 dissolves immediately into solution (within the media) while aiding wetting of any immiscible ITZ domains. Additionally, having the ITZ in an amorphous state contributes to the dissolution process by largely removing the crystalline heat of fusion and raising the solubility. However, a carrier is needed along with the amorphous API in order to achieve delayed release, sustained release or extended release. Consequently, if an API is only partially miscible in an enteric solid dispersion, localized regions of API near the particle surface could dissolve rendering the delayed release preference unfavorable. Therefore, it is critical to determine the effect of API miscibility on these modified release systems.

MDSC analysis for the URF micronized powders revealed T_g's which correlated very closely to predicted T_g's estimated from the Gordon–Taylor equation for all ITZ potency levels, solids loadings, and polymer type. Thus the API domains are too small to produce a separate T_g peak. The API may be molecularly dispersed with the polymer or the domains may be smaller than about 50 nm. Rapid freezing technologies can produce powders with nanoparticle domains as small as 20 nm in diameter (Rogers et al., 2003). The rapid freezing arrested particle growth and inhibited phase separation.

A variety of methods exist to assess miscibility limits within polymers (Eerikainen et al., 2004b; Six et al., 2003; Van den Mooter et al., 2001). For nanoparticles produced using the aerosol flow reactor method, Eerikäinen et al. determined the level at which a crystalline melting endotherm was observed for the APIs ketoprofen and naproxen. The endotherm indicates that the API solubility limit within the polymer was exceeded (Eerikainen et al., 2004a,b). Because this process involved heat to evaporate solvent, evaporation rates could be sufficiently slow to allow crystallization of the API during phase separation. Since no melting endotherms were observed for samples with 60% ITZ potency or lower, ITZ miscibility within both HP-55 and L100-55 is at least 60%. The experimental miscibility limit of ITZ in L100-55 was unexpected since ITZ miscibility levels with a structurally similar polymethacrylate polymer, Eudragit® E100, was measured at 13% (Six et al., 2002). In addition, Six et al. investigated the miscibility of ITZ with the hydrophilic polymer Eudragit® E100 and found that "cold crystallization", a recrystallization exotherm at about 133 °C was indicative of regions of pure amorphous ITZ. Investigation of total heat flow profiles for the URF powders greater than 60% ITZ revealed recrystallization exotherms indicating cold crystallization into pure itraconazole for compositions 80% ITZ and greater. Therefore it is determined that for URF micronized powders containing ITZ and either HP-55 or L100-55, the partial miscibility of the ITZ occurs between 60% and 80%, more likely occurring between 70% and 80% ITZ.

Six et al. investigated phase separation as a function of T_g by comparing the measured T_g of the solid dispersion to that of the predicted Gordon–Taylor equation. Deviations from the predicted value indicate possible partial miscibility. Also, multiple T_g's indicate phase separation or partial miscibility is occurring. For instance, the composition 4:1HP55 (2%) showed a slight transition at 60.3 °C (T_g near pure ITZ) and a larger transition at 74.7 °C providing further evidence of partial miscibility at 80% ITZ potency.

4.2. Modeling kinetics of compositions under sink and supersaturated conditions

In acidic media, the enteric polymer is insoluble and ITZ release can only occur via diffusion through the polymer, assuming the system is completely miscible and no cracks or pores within the polymer exist. Therefore, the dissolution release kinetics were modeled using the simplified Higuchi model which describes drug release as a diffusion process based on Fick's law resulting in $t^{1/2}$ dependence (Costa et al., 2001).

Drug release kinetics were modeled using the Higuchi square root model for ITZ. It was assumed that the system was planar and the matrix was homogeneous, since ITZ was completely miscible with the polymer at low concentrations. The release is described by (Higuchi, 1963):

$$Q_t = \sqrt{Dt(2A - C_s)C_s} \quad (3)$$

where Q_t is the amount of ITZ released in time t per unit area, D is the diffusion coefficient, A is the total amount of drug present in the matrix per unit volume, and C_s is the solubility of the drug in the matrix substance. Eq. (3) can be expressed as the simplified Higuchi equation:

$$Q_t = K_h t^{1/2} \quad (4)$$

where K_h is the Higuchi diffusion-related parameter. The linear fit of the data suggested that the mechanism of diffusion through the polymer matrix is consistent with the data. Other kinetic models such as zero-order release and first order release gave poor fits of the data. Only the Higuchi square root model for diffusion through the matrix offered acceptable correlation coefficients ($R^2 > 0.99$) for ITZ release under acidic conditions. Eerikäinen et al. was able to accurately predict diffusional drug release of ketoprofen from an enteric solid dispersion using the Higuchi square root model. Total ketoprofen release was estimated based on calculating the diffusion penetration depth in a 100 nm particle and the concentration of ketoprofen from within the nanoparticle (Eerikainen et al., 2004b).

The plots based on the Higuchi square root model in Fig. 7b reveal much less accurate fits for the high potency compositions ($R^2 < 0.94$) indicating a release mechanism other than diffusion through the matrix occurs during the initial phase of dissolution. Based on the MDSC data it is predicted that the ITZ within the high potency compositions existed in a partially miscible state having domains rich in ITZ, and also a significant amount of ITZ at the miscibility limit dissolved within the polymer. The MDSC data confirmed the possibility of ITZ rich regions by revealing recrystallization exotherms. Amorphous ITZ rich domains could readily dissolve within the acidic media because of their lower heat of solution and higher apparent solubility resulting in higher drug release rates during the initial phase of dissolution. The dissolution of the ITZ rich domains could also create pores and channels for additional dissolution of ITZ rich domains within the core of the particle leading to higher percentages of ITZ dissolved. This possibility is supported by the dissolution profiles since they showed faster release rates in the first 45 min compared to the final hour and 15 min. After dissolution of the ITZ rich domains, diffusion of ITZ from the polymer could continue to cause drug release, but at a slower rate as observed. In fact, modeling of the final three time points using the Higuchi model show a linear fit ($R^2 > 0.99$) suggest possible diffusion kinetics after the ITZ rich domains have dissolved. However, more data points would need to be measured to confirm this as a possible mechanism.

5. Conclusion

Particles composed of ITZ and enteric polymer were designed by ultra rapid freezing to determine the importance of composition parameters such as ITZ:polymer ratio, enteric polymer type, and particle structure on modified drug release systems. MDSC data revealed the ITZ solubility/miscibility limit within the enteric polymers HP-55 and L100-55 and were between 60 and 70% ITZ. Completely miscible low potency (20% ITZ) and partially miscible high potency (80% ITZ) high surface area powders, prepared using the URF process, were found to be

amorphous. Compositions from 2% solids loading appeared to be a highly porous matrix structure while 0.2% solids loading created nanostructured domains. For dissolution studies conducted at sink conditions in acid (i.e. non-eroding polymer condition), the matrix diffusion of ITZ in completely miscible low potency powders showed Higuchi square root kinetics, while partially miscible high potency powders exhibited additional diffusional mechanisms. Supersaturation dissolution studies, following USP guidelines for enteric release, were highly complimentary to the sink dissolution studies. All low potency compositions produced very high $C/C_{eq_{max}}$ ranging from 15- to 19-times the equilibrium value, but the high saturation driving force produced rapid precipitation. Relative to these compositions, the lower $C/C_{eq_{max}}$ levels for all high potency compositions produced less precipitation, as shown in the greater cumulative supersaturation over time. The behavior of the dissolution, under both sink and supersaturated conditions for these enteric solid dispersions is strongly influenced by the ITZ:polymer ratio, and to a lesser extent, the degree of polymer-API miscibility.

Acknowledgements

The authors kindly acknowledge the financial support from The Dow Chemical Company. Kirk A. Overhoff is a continuing American Fellowship for Pharmaceutical Education (AFPE) Fellow from 2004 to 2006 and a 2005–2006 University Continuing Fellowship recipient.

References

Costa, P., Manuel, J., Lobo, S., 2001. Modeling and comparison of dissolution profiles. Eur. J. Pharm. Sci. 13, 123–133.

Craig, D.Q.M., 2002. The mechanisms of drug release from solid dispersions in water-soluble polymers. Int. J. Pharm. 231, 131–144.

Eerikainen, H., Kauppinen, E.I., Kansikas, J., 2004a. Polymeric drug nanoparticles prepared by an aerosol flow reactor method. Pharm. Res. 21, 136–143.

Eerikainen, H., Peltonen, L., Raula, J., Hirvonen, J., Kauppinen, E.I., 2004b. Nanoparticles containing ketoprofen and acrylic polymers prepared by an aerosol flow reactor method. AAPS PharmSciTech, 5.

Frei, B.L., 2003. Investigation of Pulmonary and Oral Delivery of Itraconazole Produced by Evaporative Precipitiation into Aqueous Solution (EPAS) and Spray Freezing into Liquid (SFL) Technology in a Murine Model. College of Pharmacy, San Antonio, The University of Texas at Austin.

Hancock, B.C., Parks, M., 2000. What is the true solubility advantage for amorphous pharmaceuticals? Pharm. Res. 17, 397–404.

Hasegawa, A., Nakagawa, H., Sugimoto, I., 1984. Solid dispersion obtained from nifedipine and enteric coating agent. 1. Dissolution behavior. Yakugaku Zasshi-J. Pharm. Soc. Jpn. 104, 485–489.

Hasegawa, A., Taguchi, M., Suzuki, R., Miyata, T., Nakagawa, H., Sugimoto, I., 1988. Supersaturation mechanism of drugs from solid dispersions with enteric coating agents. Chem. Pharm. Bull. 36, 4941–4950.

Higuchi, T., 1963. Mechanism of sustained-action medication. J. Pharm. Sci. 52, 1145–1149.

Hoeben, B.J., Burgess, D.S., McConville, J.T., Najvar, L.K., Talbert, R.L., Peters, J.I., Wiederhold, N.P., Frei, B.L., Graybill, J.R., Bocanegra, R., Overhoff, K.A., Sinswat, P., Johnston, K.P., Williams, R.O., 2006. In vivo efficacy of aerosolized nanostructured itraconazole formulations for prevention of invasive pulmonary aspergillosis. Antimicrob. Agents Chemother. 50, 1552–1554.

Kai, T., Akiyama, Y., Nomura, S., Sato, M., 1996. Oral absorption improvement of poorly soluble drug using solid dispersion technique. Chem. Pharm. Bull. 44, 568–571.

Kohri, N., Yamayoshi, Y., Xin, H., Iseki, K., Sato, N., Todo, S., Miyazaki, K., 1999. Improving the oral bioavailability of albendazole in rabbits by the solid dispersion technique. J. Pharm. Pharmacol. 51, 159–164.

Kondo, N., Iwao, T., Hirai, K., Fukuda, M., Yamanouchi, K., Yokoyama, K., Miyaji, M., Ishihara, Y., Kon, K., Ogawa, Y., Mayumi, T., 1994. Improved oral absorption of enteric coprecipitates of a poorly soluble drug. J. Pharm. Sci. 83, 566–570.

Mackellar, A.J., Buckton, G., Newton, J.M., Orr, C.A., 1994. The controlled crystallization of a model powder. 2. Investigation into the mechanism of action of poloxamers in changing crystal properties. Int. J. Pharm. 112, 79–85.

Mayersohn, M., 2002. Principles of drug absorption. In: Banker, G.S., Rhodes, C.T. (Eds.), Modern Pharmaceutics, 4th ed. Marcel Dekker, Inc., New York, NY.

McConville, J.T., Overhoff, K.A., Sinswat, P., Vaughn, J.M., Frei, B.L., Burgess, D.S., Talbert, R.L., Peters, J.I., Johnston, K.P., Williams, R.O., 2006. Targeted high lung concentrations of itraconazole using nebulized dispersions in a murine model. Pharm. Res. 23, 901–911.

Nakamichi, K., Nakano, T., Yasuura, H., Izumi, S., Kawashima, Y., 2002. The role of the kneading paddle and the effects of screw revolution speed and water content on the preparation of solid dispersions using a twin-screw extruder. Int. J. Pharm. 241, 203–211.

Peeters, J.P.N., Tollenaere, J.P., Remoortere, P.V., Brewster, M.E., 2002. Characterization of the interaction of 2-hydroxypropyl-bcyclodextrin with itraconazole at pH 2,4, and 7. J. Pharm. Sci. 91, 1414–1422.

Raghavan, S.L., Kiepfer, B., Davis, A.F., Kazarian, S.G., Hadgraft, J., 2001a. Membrane transport of hydrocortisone acetate from supersaturated solutions; the role of polymers. Int. J. Pharm. 221, 95–105.

Raghavan, S.L., Trividic, A., Davis, A.F., Hadgraft, J., 2001b. Crystallization of hydrocortisone acetate: influence of polymers. Int. J. Pharm. 212, 213–221.

Rogers, T.L., Overhoff, K.A., Shah, P., Santiago, P., Yacaman, M.J., Johnston, K.P., Williams, R.O., 2003. Micronized powders of a poorly water soluble drug produced by a spray-freezing into liquid-emulsion process. Eur. J. Pharm. Biopharm. 55, 161–172.

Rowe, R.C., Sheskey, P.J., Weller, P.J. (Eds.), 2003. Handbook of Pharmaceutical Excipients. Pharmaceutical Press, London.

Sato, T., Okada, A., Sekiguchi, K., Tsuda, Y., 1981. Difference in physico-pharmaceutical properties between crystalline and noncrystalline 9,3″-diacetylmidecamycin. Chem. Pharm. Bull. 29, 2675–2682.

Sertsou, G., Butler, J., Hempenstall, J., Rades, T., 2003. Physical stability and enthalpy relaxation of drug-hydroxypropyl methylcellulose phthalate solvent change co-precipitates. J. Pharm. Pharmacol. 55, 35–41.

Sherwood, L., 2004. Human Physiology: From Cells to Systems. Thomson Learning, Belmont.

Sinswat, P., Gao, X., Yacaman, M.J., Williams III, R.O., Johnston, K.P., 2005. Stabilizer choice for rapid dissolving high potency itraconazole particles formed by evaporative precipitation into aqueous solution. Int. J. Pharm. 302, 113–124.

Six, K., Leuner, C., Dressman, J., Verreck, G., Peeters, J., Blaton, N., Augustijns, P., Kinget, R., Van den Mooter, G., 2002. Thermal properties of hot-stage extrudates of itraconazole and eudragit E100: phase separation and polymorphism. J. Therm. Anal. 68, 591–601.

Six, K., Murphy, J., Weuts, I., Craig, D.Q.M., Verreck, G., Peeters, J., Brewster, M., Van den Mooter, G., 2003. Identification of phase separation in solid dispersions of itraconazole and Eudragit (R) E100 using microthermal analysis. Pharm. Res. 20, 135–138.

Six, K., Verreck, G., Peeters, J., Brewster, M., Van den Mooter, G., 2004. Increased physical stability and improved dissolution properties of itraconazole, a class II drug, by solid dispersions that combine fast- and slow-dissolving polymers. J. Pharm. Sci. 93, 124–131.

Sung, M.H., Kim, J.S., Kim, W.S., Hirasawa, I., 2002. Modification of crystal growth mechanism of yttrium oxalate in metastable solution. J. Cryst. Growth 235, 529–540.

Suzuki, H., Sunada, H., 1998. Influence of water-soluble polymers on the dissolution of nifedipine solid dispersions with combined carriers. Chem. Pharm. Bull. 46, 482–487.

Takeuchi, H., Handa, T., Kawashima, Y., 1987. Spherical solid dispersion containing amorphous tolbutamide embedded in enteric coating polymers or colloidal silica prepared by spray-drying technique. Chem. Pharm. Bull. 35, 3800–3806.

Van den Mooter, G., Wuyts, M., Blaton, N., Busson, R., Grobet, P., Augustijns, P., Kinget, R., 2001. Physical stabilisation of amorphous ketoconazole in solid dispersions with polyvinylpyrrolidone K25. Eur. J. Pharm. Sci. 12, 261–269.

Varshosaz, J., Kennedy, R.A., Gipps, E. M., 1997. Use of enteric polymers for production of microspheres by extrusion-spheronization. 72, 145–152.

Yamashita, K., Nakate, T., Okimoto, K., Ohike, A., Tokunaga, Y., Ibuki, R., Higaki, K., Kimura, T., 2003. Establishment of new preparation method for solid dispersion formulation of tacrolimus. Int. J. Pharm. 267, 79–91.

Yoshihashi, Y., Kitano, H., Yonemochi, E., Terada, K., 2000. Quantitative correlation between initial dissolution rate and heat of fusion of drug substance. Int. J. Pharm. 204, 1–6.